Studies of the Cosmic Ray shadow of the Moon using the KM3NeT/ARCA telescope

Kingma, Tjalling

Studies of the Cosmic Ray shadow of the Moon using the KM3NeT/ARCA telescope

THESIS

submitted in partial fulfillment of the
requirements for the degree of

BACHELOR OF SCIENCE
in
PHYSICS

Author :	T.M. Kingma
Student ID :	2648490
Supervisor :	Dr. D.F.E. Samtleben
2^{nd} corrector :	Dr. M.J.A. de Dood

Leiden, The Netherlands, July 2, 2024

Studies of the Cosmic Ray shadow of the Moon using the KM3NeT/ARCA telescope

T.M. Kingma

Huygens-Kamerlingh Onnes Laboratory, Leiden University
P.O. Box 9500, 2300 RA Leiden, The Netherlands

July 2, 2024

Abstract

Cosmic rays produce muons that cast Cherenkov light cones in the water. With the Cherenkov light cones, KM3NeT can reconstruct the track of the muon across the sky, this result is named an event. Between September 22 2022 GMT and June 09 2023 GMT, the ARCA site was measuring, and detecting Cherenkov light from any bypassing muon. From this measurement simulations were created, containing 6 times more events as the measurement. In this thesis, we analyse the events from the simulation. We bin the events on one- & two-dimensional maps of the sky, where we bin all reconstructed events relative to the location of the Moon. Two models are fitted to the maps. One model assumes the absence of the Moon; another model respects a valley in events at the Moon's location. These fits are tested with the use of χ^2-tests. The one-dimensional analysis indicates a relative amplitude of 0.65 ± 0.10 and angular resolution of $0.81^\circ \pm 0.12^\circ$. The rotational calibration of the telescope is tested. Although the χ^2 values differ most for no rotational calibration an angle of -0.2 and -0.4 are larger than expected. Quality cuts of the data set are based on the variables' likelihood and track reconstruction uncertainty. It is the superposition of a likelihood of 100 or higher and a track reconstruction uncertainty of 0.1 or smaller that causes an increase in the difference in χ^2 values.

Contents

Version of July 2, 2024– Created July 2, 2024 - 13:46

Chapter 1

Introduction

1.1 Cosmic rays atmosphere interaction

The Earth gets bombarded by cosmic rays from all directions. Cosmic rays are a mixture of nuclei and charged subatomic particles but predominantly consist of protons. These rays collide with the Earth's upper atmosphere. This interaction results in the creation of a pion π, which can decay into two different particles, one of them being a neutrino ν_μ. The other resulting particle of this process is the muon $\mu^{+/-}$. An example of such atmospheric collision, resulting in a muon and a muonic neutrino, is equation (1.1), where a proton from the cosmic rays collides with a stable Nitrogen molecule at the top of the atmosphere.

$$p^+ + N_2 \rightarrow \pi^{+/-} \rightarrow \mu^{+/-} + \nu_\mu \tag{1.1}$$

The muons travel through the atmosphere to eventually reach the Earth's surface or bottom of the seas. Below the sea surface, they can be detected by an underground or underwater muon detector. KM3NeT/ARCA telescope is one such underwater telescope. The Moon and the Sun are two celestial objects that can stand in the pathway of cosmic rays. These objects should cast a shadow of the muons measured on Earth.

1.2 Purpose of study

This study analysed the data received from the KM3NeT/ARCA telescope and attempted to identify the blockage of measured muons (events) caused by the presence of the Moon. In other words, we are trying to find the

shadow that the Moon casts over the Earth in the cosmic bombardment of Cosmic Rays.

In the one-dimensional analysis, we bin in radii from the Moon and thus one step in a larger radius is one bin. In the one-dimensional analysis, we search for the amplitude of the shadow and the width σ_{res} of the Moon's shadow.

In the two-dimensional analysis, we primarily locate the position of the Moon with the χ^2-tests onto the fits. We will also test the KM3NeT's rotational calibration by assuming it is incorrect. In the two-dimensional analysis, there will also be quality cuts made to the data to filter out poorly reconstructed events.

Chapter 2

KM3NeT/ARCA

2.1 KM3NeT

KM3NeT is a research framework constructed by European collaboration. The KM3NeT telescopes consist of building blocks of highly sensitive optical detectors in 3D arrays, with a total volume of a cubic kilometre. That is the reason behind its name (KM^3 Neutrino Telescope). These telescopes are placed in the Mediterranean Sea.

2.2 ARCA

There are currently two sites. Namely ORCA and ARCA. These are acronyms for: 'Oscillation Research with Cosmics in the Abyss' and 'Astro-particle Research with Cosmics in the Abyss'. The two telescopes are calibrated for different energy regimes for the neutrino. ORCA is meant to detect neutrinos from the atmospheric interaction of the cosmic ray.[1] ARCA is meant to detect neutrinos from the depths of the universe.[1] ARCA is meant to measure neutrinos within the energy range of $10^2 \div 10^8$ GeV [2]. The ARCA site is located at offshore Capo Passero, Sicily, Italy at the bottom of the Mediterranean Sea[**ARCApotential**].

2.3 DUs & DOMs

At the time of measurement, ARCA had 21 Detection Units (DU). These detection units consist out of 700-metre double optical fibre with 18 Digital Optical Modules (DOMs) distributed with a distance of 36 metres be-

tween them [3][4][5]. DOMs are the optical sensors of the neutrino telescope. Each DOM has 31 photomultiplier tubes (PMTs), and all PMTs are connected to the central control unit named the octopus[5]. The fibre is mounted onto the seabed 3.5 kilometres deep [4].

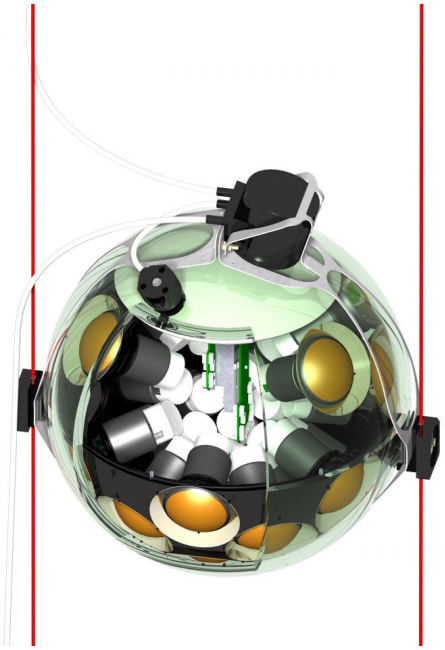

Figure 2.1: *Copyright KM3NeT [6]; Inside of a DOM. 31 PMTs (orange) connected to the octopus (green) within the glass vessel connected by optical fibres.*

2.4 Track reconstruction

When muons travel through seawater they cast Cherenkov light. This light is detected by multiple DOMs from different angles and with correlated timestamps. The algorithm will use a best-track hypothesis, which means it will assume there is a track that matches best with the observed hit pattern from different DOMs. This reconstructed track will be optimised with a fit maximising the likelihood of the corresponding hit pattern. This fitting to optimise for the maximum likelihood of the event, results in an uncertainty of direction of the track. This uncertainty β, is in units of degrees. The total information of the muon track reconstruction and its direction is named an event.

Chapter 3

Data from ARCA21

This research analyses a simulation dataset. This simulation corresponds well with the real dataset. The real dataset measurement collection started on Thursday, September 22nd, 2022, at 17:03 and ended on Saturday, June 10th, 2023, at 01:59 (Central European Summer Time). During the time of measurement, the ARCA telescope had 21 strings with DOMs attached to them.

In the data sets, every row is one event. Every event has multiple columns of variables. Significant variables for this research are:

1. r: relative distance to the Moon
2. x: azimuth distance to the Moon
3. y: elevation distance to the Moon
4. lik: likelihood of the event
5. β: track reconstruction uncertainty
6. angular resolution: the angular resolution of the event.

r,x,y are all in units of degrees. Likelihood is the likelihood of fit of the reconstructed track being optimised for corresponding to the observed Cherenkov light at the triggered timestamps. Beta is the uncertainty of the direction of the reconstructed track in radians.

3.1 Monte Carlo simulation

The Monte Carlo simulation has an extra variable, namely the angular resolution. The angular resolution is found by, together with the likelihood and track reconstruction uncertainty, will be used to make quality cuts of the data of the simulation. In this study, we will primarily analyse the Monte Carlo simulation. Monte Carlo simulations have been proven to be reliable and correspond well with the actual collected measurements [2].

Version of July 2, 2024– Created July 2, 2024 - 13:46

Chapter 4

Analysis method

The events are described as a phase space of the angular distance between the reconstructed path of the muon and the direction of the Moon. These are conducted as a one-dimensional relative distance and a two-dimensional distance that is dispersed into an elevation distance and an azimuth distance.

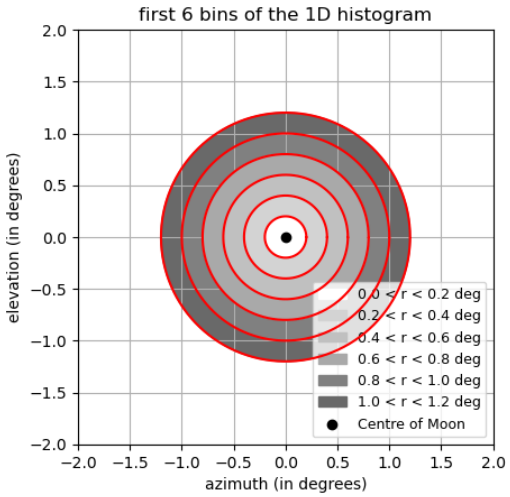

Figure 4.1: *Visualisation of the one-dimensional bins. Here are shown the first 6 bins of the histogram. The bins do not have the same surface, which has to be normalised with the area defined in equation* (4.1).

The bins must be normalised as there will be an offset for the higher angle valued bins. If one assumes an isotropic event distribution, higher-valued bins will have more events. For the one-dimensional case, an isotropic distribution of events is justified, unlike the two-dimensional case as we

will see. To normalise the bins, we divide them by their area. θ_1 is one bin larger than θ_2.

$$Area = 360^\circ(cos\theta_2 - cos\theta_1) \tag{4.1}$$

With the normalisation, the units of the bins are now $events \times degree^{-2}$. The definition in equation (4.1) comes from the fact that we want to find a surface on a sphere [*].

This sphere is the sky from the perspective of the telescope. Just as the Sun/Moon shadows were found with the ORCA telescope, the background model is compared to a model with a negative Gaussian expected by the shadow of the Moon. When the histogram is created, with the x-axis the bins and the y-axis the amount of events, we fit two functions. One function is the average. The other function is a Gauss function subtracted from the background average.

We assume that the shadow of the Moon is shaped as a Gaussian function based on approximations. The first approximation is that the size of the Moon is neglected. This approximation is valid, as long as the angular resolution of the detector is larger than the angular radius of the Moon [7]. This is the case in this study. The Gaussianity is a first-order approximation.

The one-dimensional model is:

$$N_{H1}^{1D} = bg - \frac{A}{\sqrt{2\pi}\sigma_{res}} e^{-\frac{r^2}{2\sigma_{res}^2}} \tag{4.2}$$

Note that the Moon is at $r = 0$, therefore no offset in the exponent is required. Equation (4.2) has fitting parameters A and bg. Where A is the amplitude of the Gauss distribution. And bg is the amplitude of the background signal, the detected muons as if there was no Moon at all. $\sigma_{res}$is the angular resolution of the detector of the event. At the start, we assume $\sigma_{res} \approx 0.8$. Later in the two-dimensional analyses, we will find the true values. We will compare the model (4.2) with the fitted average $N_{H0} = bg$.

The two-dimensional analysis uses two axes: $X = (\phi_{☾} - \phi_{event}) \times sin(\theta_{event})$ and $Y = \theta_{☾} - \theta_{event}$. Where $\phi_{event}, \theta_{event}$ are the azimuth and elevation angles of the reconstructed track event. And $\phi_{☾}, \theta_{☾}$ are the azimuth and elevation angle of the Moon.

As the elevation angle Y becomes larger, more events are received per $degree^2$. The expected background is therefore no longer a constant as in the one-dimensional case, but rather taken as a second-order polynomial:

[*]Note that with use of a Taylor expansion, for small θ the area becomes: $Area = \pi\theta_1^2 - \pi\theta_2^2$. This is a simple flat surface situation. This approximation is valid if we look very close to the zenith.

Version of July 2, 2024– Created July 2, 2024 - 13:46

$$N_{i,H0} = \rho(1 + a_1 y_i + a_2 y_i^2) \tag{4.3}$$

Where ρ is the background amplitude parameter and a_1, a_2 are the respected parameters for the powers of the polynomial.

The two-dimensional background model becomes:

$$N_{H1}^{2D} = \rho \left[1 + a_1 y_i + a_2 y_i^2 - A \frac{R_{\leftmoon}^2}{2\sigma_{res}^2} e^{-\frac{(x-x_0)^2+(y-y_0)^2}{2\sigma_{res}^2}} \right] \tag{4.4}$$

Where x_0, y_0 are the centre of the fitted function. The two-dimensional background function (4.3) as well as our model (4.4) is similarly defined as in KM3NeT/ORCA first observation [7].

σ_{res} is found as we allow for the one-dimensional model 4.2 to be fit for parameters: bg, A and σ_{res}. That being said, it should be noted that in this one-dimensional binning, information is lost. An instance of this loss of information is the background distribution. The background is assumed and taken to be a constant. But as we will see in the results 5, this is not the case once we arrive at the two-dimensional analysis.

4.1 Relative amplitude & σ_{res}

The two surfaces of the integral of the Gaussian function in equation (4.2) and the surface of the expected missing events, can be rewritten as a fraction, we call the fraction the relative amplitude.

Reminding both bg and A are in units of $events \times degree^{-2}$, one can calculate the expected amplitude by multiplying the surface of the Moon with the background density events. $A_{expected} = bg$. With the radius of the Moon $R_{\leftmoon} = 0.26\,^{\circ}$as taken in many other previous observatories such as KM3NeT/ORCA, IceCube, ANTARES and many more [7][8][9]. This combines in an expected amount of missed events: $\Omega_{expected} = bg(1 - cos(R_{\leftmoon}))$, where we take the area of the Moon in the sky (equation (4.1) with $\theta_2 = 0$). It should be noted that the expected amplitude $\Omega_{expected}$ is in units of $events$ and A_{fit} in $events \times degree^{-2}$. Thus we will also introduce a total amount of missed events according to the fit: Ω_{fitted}. Here we define Ω_{fitted} as:

$$\Omega_{fitted} = A_{fit} \times \int_0^{\infty} \frac{1}{\sqrt{2\pi}\sigma} e^{-\frac{r_{fit}^2}{2\sigma^2}}\, dr_{fit} \tag{4.5}$$

The Gaussian integral is normalised. We define the relative amplitude as a unitless fraction of the expected missed events:

Version of July 2, 2024– Created July 2, 2024 - 13:46

$$A_{rel} = \frac{\Omega_{fitted}}{\Omega_{expected}} = \frac{A_{fit}/2}{bg \times (1 - cos(R_{☾}))} \tag{4.6}$$

We are interested in the relative amplitude, as this may sign the significance of the reduction in amplitude. A high relative amplitude is a reason to continue the investigation and show that this is not just a statistical deviation in the distribution of the event, but rather a shadow of an object.

4.2 $\Delta\chi^2$ analysis

For both the one- as the two-dimensional analyses will the respected χ^2 values of the fit of the model with the Gaussian valley be compared with the χ^2 of the background, hence we introduce $\Delta\chi^2$ for both the one- as the two-dimensional analyses. From these values, the difference can be found:

$$\Delta\chi^2 = \chi^2_{N_{H0}} - \chi^2_{N_{H1}} \tag{4.7}$$

Here is $\chi^2_{N_{H0}}$ corresponding with the χ^2 value of the average in the one-dimensional analysis, and the background model (4.3) in the two-dimensional analysis. $\chi^2_{N_{H1}}$ corresponds to the χ^2-value of the one-dimensional model (4.2) or the two-dimensional model (4.4). This value tells us how much better the model N^{1D}_{H1} (4.2) fits than the average. The value of $\chi^2_{N_{H1}}$ must not be too large. For $\Delta\chi^2$ a positive value is expected as the model has an extra parameter to make the fit suit the data better. Mind that setting the amplitude A to zero returns the average N_{H0} definition. The model has therefore an extra dimension to perform a better fit.

In the case of the two-dimensional analysis, the events will be binned in a 2-dimensional histogram for different values of X, and Y. The model will be the background with a two-dimensional Gaussian function subtracted from the background. The two-dimensional analysis will differ from the 1 dimensional by assuming every bin is the Moon's centre and thus calculating the chi-squared value of the model being centred at every bin. The χ^2-value of the model around (0,0) should be much smaller than that of the background model. And at bins far away from (0,0), the χ^2-value of the model should be close or equal to that of the background model.

Version of July 2, 2024– Created July 2, 2024 - 13:46

4.3 Rotational calibration

So far we have assumed that the rotational calibration of the telescope is correct. To test that the azimuth direction is really the azimuth direction, we will assume the telescope is positioned incorrectly with an interval of $-2^\circ \leq \alpha \leq 2^\circ$, with α the assumed rotational miscalibration in degrees.

From here we will calculate the $\Delta\chi^2_{(0,0)}$, which is the delta chi-squared value at (0,0) for (X', Y'), with Y' = Y:

$$X' = X + \alpha cos(Y) \tag{4.8}$$

The azimuth events are summed with an additional rotation times the cosine of the elevation. We will fit the model (4.4) and the background function (4.3) and find $\Delta\chi^2_{(0,0)}$ and $\chi^2_{(0,0)}$ of the model 4.4 for all values within this interval with a step size of 0.2. We expected the telescope to be well rotational calibrated. If this is the case, the $\Delta\chi^2_{(0,0)}$, at $\alpha = 0$ should be larges. and drop off as α deviates from zero. Also χ^2_{model} should be smallest at $\alpha = 0$.

4.4 Angular resolution (Quality-cut)

The data that we use here is a simulation containing 6 times more events than the measurement. Some of these events are poorly reconstructed or have a low angular resolution. Including these events in the analysis methods will reduce the precision of the fits. With the use of quality cuts, we attempt to exclude these events.

To perform such quality cuts, use two cut variables:

1. lik: Likelihood value of the track reconstruction

2. β: directional uncertainty of the track reconstruction.

Each event has a value for these two cut variables. We perform quality cuts of the data set based on these two variables, as these two variables tell us about the quality of their track reconstruction. We will use 6 different values for both the likelihood and the track reconstruction uncertainty, resulting in 36 combinations. For each combination of likelihood (lik) and uncertainty β, we will cut the data set and include only the events for which the likelihood is equal or larger than the conditioned cut value and the uncertainty equal or smaller than the conditioned cut value.

Each event has a value for the variable 'angular resolution'. Each quality cut will have the median angular resolution calculated. We take the median angular resolution of the quality cut as the value σ_{res}. Each quality cut will be fitted with 4.4, with the value of σ_{res} calculated from that quality cut.

We then will find the $\Delta\chi^2_{(0,0)}$ and $\chi^2_{(0,0)}$, using only the events in their respective quality cut and their corresponding σ_{res}. From these quality cuts, we can find for each (lik, β) combination, the value of σ_{res}, $\Delta\chi^2_{(0,0)}$ and $\chi^2_{(0,0)model}$.

Chapter 5

Data analysis results

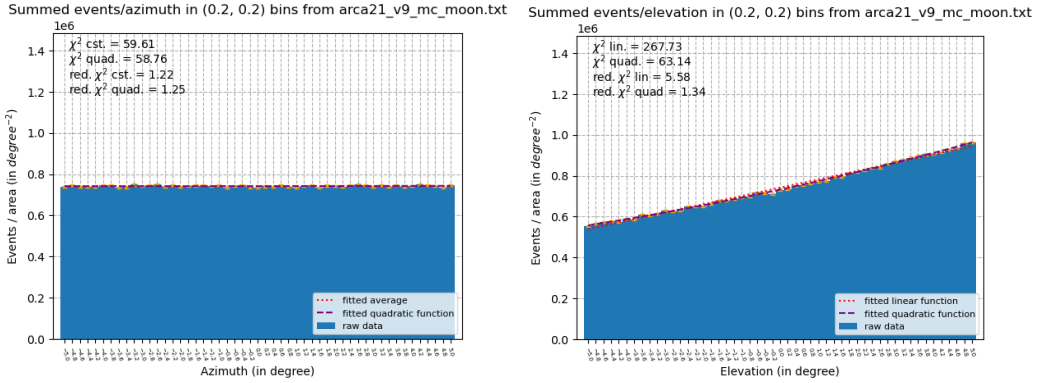

(i) *An azimuth side view of the two-dimensional histogram, with a fitted average and a fitted order two polynomial.*

(ii) *An elevation side view of the two-dimensional histogram, with a fitted linear function as a fitted order two polynomial.*

Figure 5.1: *Summed side views of the two-dimensional histogram.*

In figure 5.1i we fit both a constant fitted average and a second-order polynomial, as we expect a small but negligible reduction at the edges. With the χ^2 values of both the fits, we can determine if the events' reduction is insignificant. The χ^2 value of the constant is 59.61 and the second-order polynomial is 58.76, this small difference between the two χ^2-values indicates that we can neglect the expected drop-off of events at ± 5 degrees in the azimuth direction.

In figure 5.1ii we fit both an order one polynomial as well as a second-order polynomial, as the elevation grows larger we see the elevation increase. The χ^2 value of the first-order polynomial is valued at 267.73 and

that of the second-order is valued at 63.14. We determine from the difference of the χ^2 values that the increase is more likely a second-order polynomial. This revelation is of great importance. It shows us that the background is not a constant but a polynomial for the elevation as expected with equation (4.3). Thus for the model, we require equation (4.4).

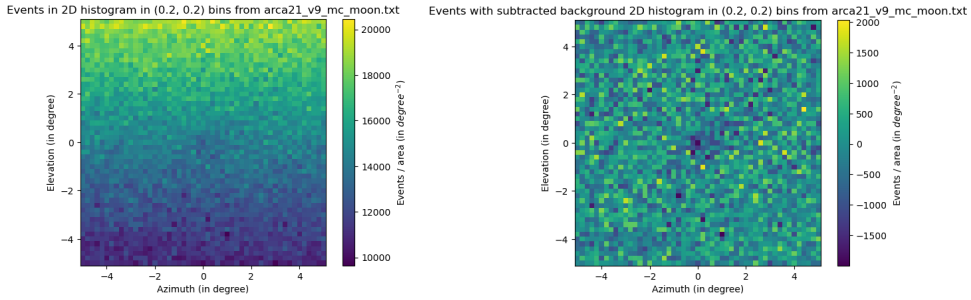

(i) *The raw data of events in each bin.*

(ii) *The data normalised with regards to the second-order polynomial.*

Figure 5.2: *The difference between the raw and normalised data.*

Figure 5.2i is the raw data, over which the background (4.3) and model (4.4) will be fitted. Figure 5.2ii is the figure with the subtracted fitted second-order polynomial. With the polynomial background subtracted, we should see only deviations such as the presence of the Moon.

5.1 Relative amplitude & σ_{res}

The relative amplitude and σ_{res} are extracted from the one-dimensional analysis, as the amplitude and the sigma are both fitting parameters.

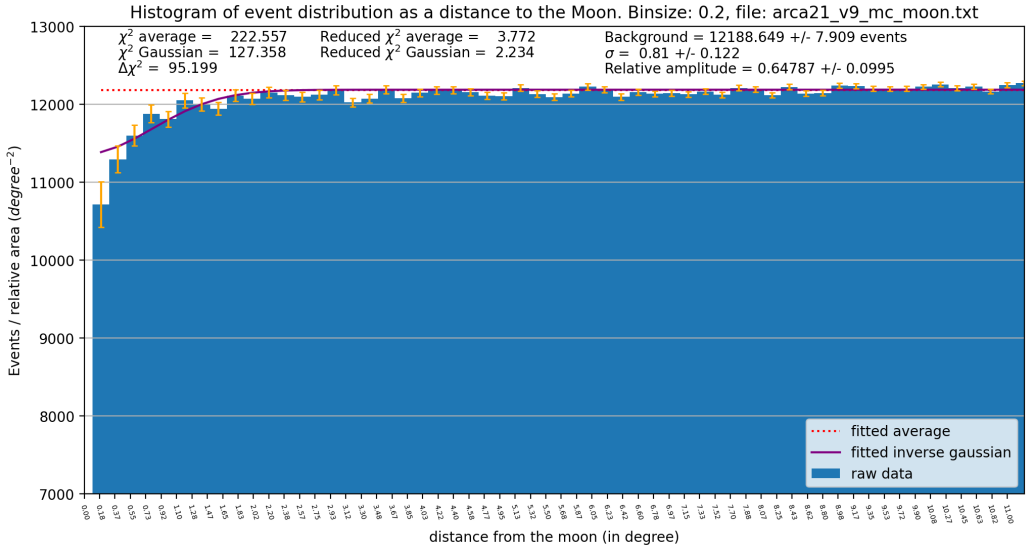

Figure 5.3: *The one-dimensional histogram of events over the relative distance to the Moon. The fitted χ^2 of the two fitted models indicate a viable reason to believe that there is a statistical valley in events at the location of the Moon.*

The value of $\sigma_{res} = 0.81^\circ \pm 0.122^\circ$. This supports the assumption for the two-dimensional analysis, which we assumed that $\sigma_{res} \approx 0.8$ degrees. As in the two-dimensional analysis, σ_{res} is a constant and not a fitting parameter. During the quality cuts will the angular resolution be recalculated for each different cut.

The relative amplitude is 0.65 ± 0.01 which is significant enough to expect an object at the location of the Moon.

We already fit all parameters in the one-dimensional model in the one-dimensional analysis. We can compare this to the two-dimensional model if we allow the two-dimensional model to also fit for all parameters. This is of interest as information is lost in the one-dimensional analysis.

We allow the one-dimensional analysis fit for the parameters: bg, A, & σ_{res}. Where bg is the background. A is the amplitude and σ_{res} is the angular resolution as described in (4.2). We can do the same thing and compare the two methods. In the two-dimensional model 4.4 we fit for the parameters: ρ, A_{rel}, σres, x_0, & y_0. Where ρ is the scaling factor in $events/degrees^2$. A is the relative amplitude. x_0, y_0 are the position of the Gaussian function.

The found parameters of the Moon:

Parameters	Moon 1D	Moon 2D
σ_{res}	$0.81^\circ \pm 0.12^\circ$	$0.53^\circ \pm 0.07^\circ$
Relative amplitude (A_{rel})	0.65 ± 0.01	0.56 ± 0.11
$\Delta\chi^2$	95.20	56.29
$events \times degree^-2$	12189 ± 8	14395 ± 19

Table 5.1: *The parameters at $(x_0, y_0) = (0, 0)$ for the one-dimensional fit and the two-dimensional fit. Allowing to fit 1d for (bg,A,σ_{res}) and 2d for: (ρ,A_{rel},σ_{res},x_0,y_0)*

The two dimensional location of the Moon (x_0, y_0) is $(0.213^\circ \pm 0.100^\circ, 0.002^\circ \pm 0.100^\circ)$. It is notable that the angular resolution of $0.53^\circ \pm 0.07^\circ$ is significantly smaller than the one-dimensional case. The fact that $\Delta\chi^2$ in the one-dimensional analysis is larger than the two-dimensional analysis, is likely correlated to the fact that the one-dimensional binning does not contain all the information.

5.2 $\Delta\chi^2$ analysis

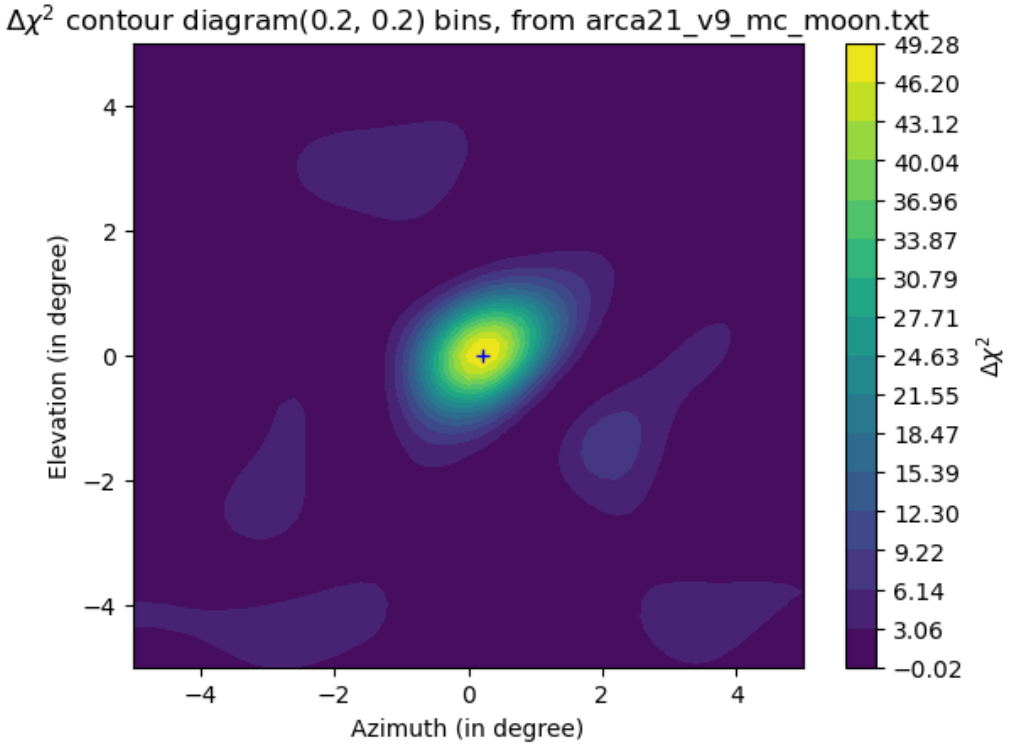

Figure 5.4: *This is a contour diagram of the $\Delta\chi^2$ values where the location of the (x_0, y_0) in model* (4.4) *is positioned at each bin.*

From figure (5.4) we determine that around the (0,0) the $\Delta\chi^2$ value is highest, valued at 49.28. This indicates that the model (4.4) is a much better fit around (0,0) than the background model (4.3). The centre of the Moon does not seem to be at (0,0), but rather at (0.2,0).

It should be noted that there are negative $\Delta\chi^2$ for some bins. This should not be statistically possible, as the only added parameter is an amplitude, which if set to zero, returns the background function. Thus $\Delta\chi^2$, as defined in equation (4.7), should always be larger or equal to zero.

Version of July 2, 2024– Created July 2, 2024 - 13:46

5.3 Rotational calibration

We made the plot for a rotational miscalculation $\alpha \in [-2, 2]$ with steps of 0.2.

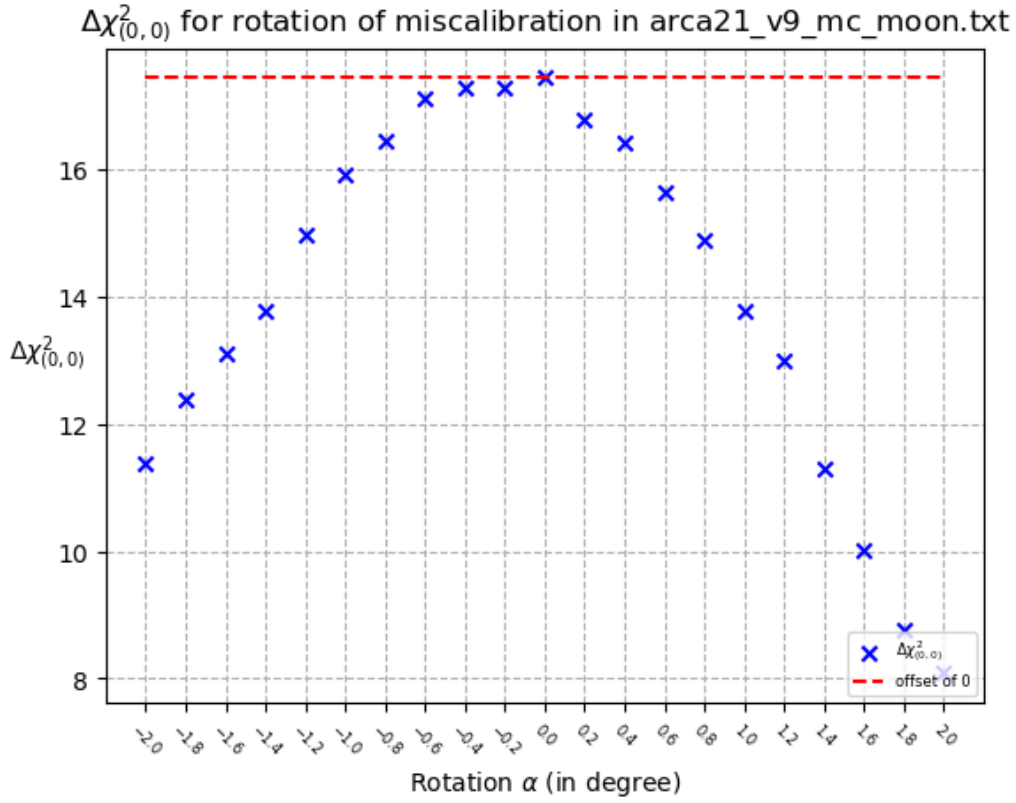

Figure 5.5: *$\Delta\chi^2$ for every step of rotational calibration α with steps of 0.2 degrees.*

From figure 5.5 we notice firstly that at $\alpha = 0$ the $\Delta\chi^2$ value is at its largest, which is as expected. That being said, we do also notice that for miscalibration of $-0.2°$ and $-0.4°$, the $\Delta\chi^2$ are still higher than expected. We expect a second-order polynomial with the peak at $\alpha = 0°$. This invites us to look at the χ^2 value of the fitted model (4.4).

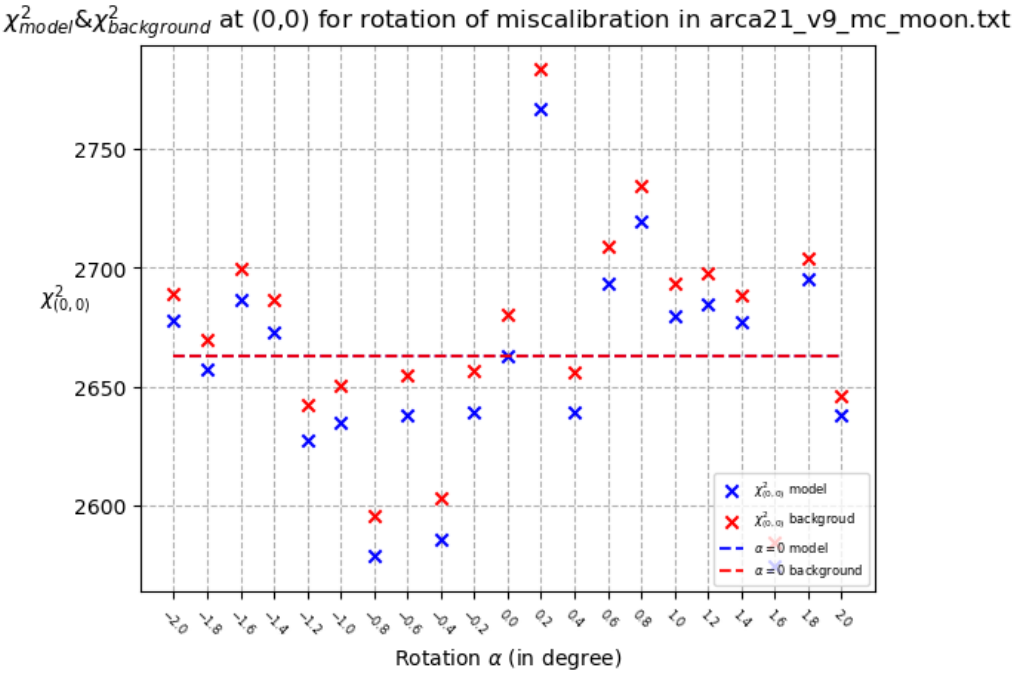

Figure 5.6: *The χ^2-values of the background model as well as the inverse Gauss model.*

We notice a dominant statistical fluctuation in figure 5.6 for all values of α within the range of $\pm 2.0^\circ$. Besides the statistical fluctuations, it is also noticeable that the χ^2 values of the model (4.4) and that of the background model (4.3) are correlated to each other. This is visible as both models obey the same statistical fluctuation in figure 5.6.

5.4 Angular resolution (Quality-cut)

The quality cuts have been made for 6 different values of likelihood and 6 different values of the track reconstruction uncertainty β. Before we can indicate the values of the conditions, we must first see the distribution between likelihood and track reconstruction uncertainty.

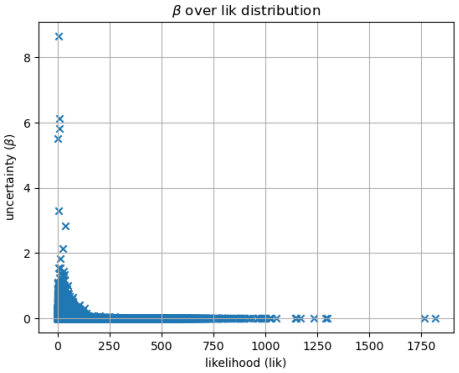

(i) *The total distribution of the likelihood and the track reconstruction uncertainty.*

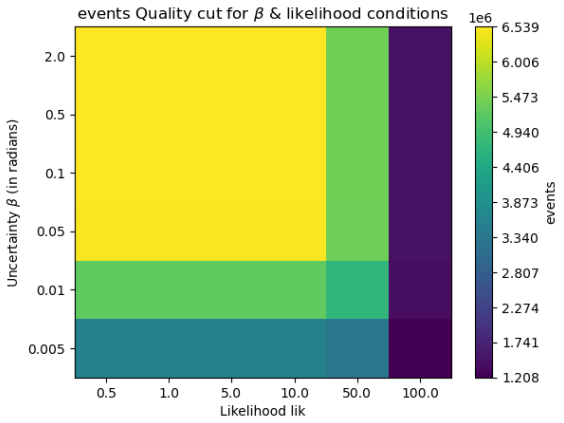

(ii) *The amount of events in each quality cut.*

Figure 5.7: *The distribution between the track reconstruction uncertainty (β) and the likelihood (lik).*

The knowledge we achieved from figure 5.7i is to find the order of magnitude of the values and with that also the starting values for the condition of the quality cuts. From figure 5.7i we notice that the majority of the likelihood is below 250, and the uncertainty is below 2°.

Figure 5.7ii shows us that the smallest bin, which is the quality cut with the highest likelihood and smallest track reconstruction uncertainty, is still in the order of millions of events. This allows us to choose the largest likelihood condition of 100 and the largest uncertainty of 2°.

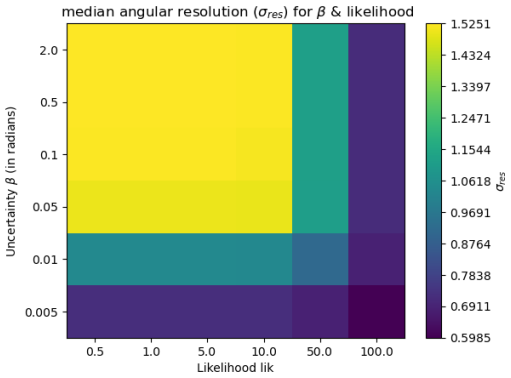

Figure 5.8: *The σ_{res}, which we have taken as the median angular resolution of the quality cut. We take σ_{res} values from the quality cut, which will be used for fitting the cut data with the model* (4.4).

From figure 5.8 we can deduce that for smaller allowed track reconstruction uncertainty and a high likelihood, the σ_{res} becomes smaller. The figure indicates that the median angular resolution is proportional to the likelihood and inversely proportional to the track reconstruction uncertainty.

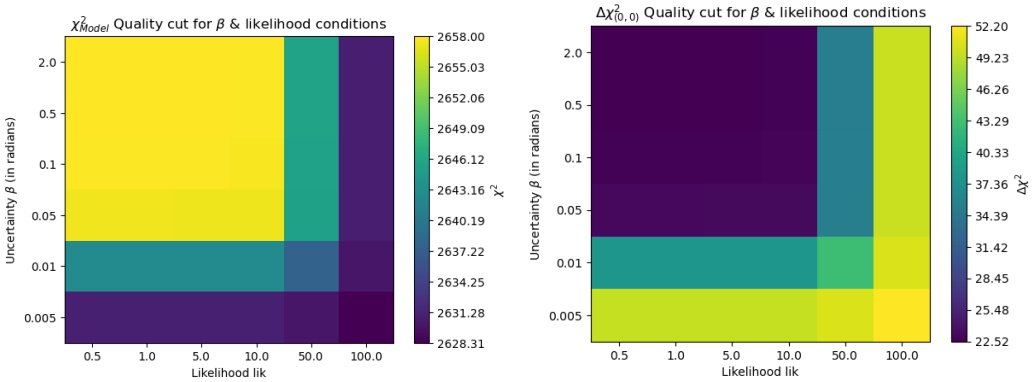

(i) *The χ^2 of the model for each quality cut.* ***(ii)*** *The $\Delta\chi^2$ value for each quality cut.*

Figure 5.9: *The χ^2 & $\Delta\chi^2$ values for every quality cut, with the Gauss function in equation* (4.4) *(x_0, y_0) centred at (0,0).*

From figure 5.9i we can deduct that the model (4.4) has a smaller χ^2 for the quality cut with the minimum likelihood of 100 and a maximum of track reconstruction uncertainty of 5×10^{-3}. Figure 5.9ii tells us that the χ^2 of the background model (4.3) does not reduce as much as the χ^2 of the model (4.4).

We expected that a higher likelihood would result in a better track reconstruction. The improved track reconstruction should cause a better angular resolution. For the uncertainty of the direction of the track reconstruction, we expect that a lower uncertainty should result in a higher angular resolution of the event. Both of these expectations are supported by the found results. We notice that for higher likelihood conditions the median angular resolution σ_{res} becomes smaller in figure 5.8. As a result, we see χ^2 of the model become smaller (see figure 5.9i) and $\Delta\chi^2$ increase (see figure 5.9ii) as the likelihood condition become stricter. The directional uncertainty of the track reconstruction shows the same trend. As the uncertainty conditions become smaller and stricter the angular resolution σ_{res} becomes smaller in figure 5.8. The result of the smaller angular resolution σ_{res} is that the χ^2 of the model reduces (see figure 5.9i and $\Delta\chi^2$ increases (see figure 5.9ii). We expected that the combination of both stricter quality cut conditions would result in a supper position of reduced angular resolution σ_{res}. In figure 5.8 we notice that it is indeed the combination of the strictest likelihood of 100 or higher and an uncertainty of 0.1° or lower. The resulting χ^2 of the model in figure 5.9i, is also lowest at the combination of the two conditions' strictest quality cut. The $\Delta\chi^2$ in figure 5.9ii is the biggest with the strictest quality cut.

Chapter 6

Conclusion

6.1 Conclusion

From the one-dimensional analysis, we found that an angular resolution of $\sigma_{res} \approx 0.8^\circ$ is a viable value. in addition, the relative amplitude from the fit clearly indicates the valley of measured events for a small distance to the Moon. From the two-dimensional analysis, we found with the use of χ^2-analysis a shadow at the position of the Moon as shown in figure 5.4. We also found that the rotational calibration of the telescope is well, except for an odd occurrence for a rotation for -0.2°and -0.4°. The quality cuts 5.4 shows us that if we filter out any impurity, and maintain only the likelihood of 100 or higher and track reconstruction uncertainty of 0.1 or lower the quality of the $\Delta\chi^2$ value significantly increases. It is the combination of both a very low track reconstruction uncertainty and a high likelihood that causes a high quality in events.

The purpose of this research was to analyse the simulation data which was based on the ARCA21 real data set measurement from 2022-2023. In this analysis, the purpose was to first find a one-dimensional indication of the Moon shadow with the use of fitting a flat model and a model with an indent. In the two-dimensional analysis, we extended the research to also test the rotational calibration of the ARCA detector site, as well as to find suitable quality cuts in the two cut variables: the likelihood and the track reconstruction uncertainty.

6.2 Discussion

The $\Delta\chi^2$ value found around the expected value of (0,0) is higher than that further away from the Moon's location. What puts the analysis in 5.2 and in particular figure 4.7 in question, is the fact that there are also negative values. That should not be the case and is likely a coding error or a lack in understanding of the data and methods used during the course of this project. In section 4.4 we used the median angular resolution of the quality cut as the angular resolution σ_{res} in the model 4.4. While these two are not the same thing. They are heavily correlated.

There are many questions yet to be answered. Future research might be able to apply deeper statistical analysis to the Monte-Carlo simulations. This research does not apply the log-likelihood function nor mentions Poisson likelihood anywhere. This study assumed a Gaussian distribution based on the approximations of previous research. Future research should also, compare complete KM3NeT/ARCA simulations with the KM3NeT/ORCA. The simulated data should also be compared to the KM3NeT/ORCA telescope to notice and investigate any difference in measurement accuracy and track reconstruction accuracy. The DOMs from the KM3NeT/ARCA telescope are further from each other located from one another than that of KM3NeT/ORCA, and therefore should have a different accuracy in the track reconstruction and the angular resolution.

6.3 Acknowledgements

I would like to express my gratitude to Dr. Dorothea Samtleben, as she supervised this BSc project. I am also grateful for the hospitality of the whole KM3NeT/neutrino team at Nikhef in Amsterdam. It was a delightful, educational and fascinating experience to witness physicists at work.

Bibliography

[1] S AdriÃ¡n-MartÃnez et al. "Letter of intent for KM3NeT 2.0." In: *Journal of Physics G: Nuclear and Particle Physics* 43.8 (June 2016), p. 084001. ISSN: 1361-6471. DOI: 10.1088/0954-3899/43/8/084001. URL: http://dx.doi.org/10.1088/0954-3899/43/8/084001.

[2] Giovanna Ferrara and Simone Biagi. "First results of the KM3NeT/ARCA detector." In: *Journal of Physics: Conference Series* 1056 (July 2018), p. 012021. DOI: 10.1088/1742-6596/1056/1/012021.

[3] Simone Biagi. "KM3NeT/ARCA: Status of construction and recent physics results." In: *EPJ Web of Conferences* 280 (Mar. 2023). DOI: 10.1051/epjconf/202328001004.

[4] S. Aiello et al. *Astronomy potential of KM3NeT/ARCA*. 2024. arXiv: 2402.08363 [astro-ph.HE].

[5] E Leonora. "The Digital Optical Module of KM3NeT." In: *Journal of Physics: Conference Series* 1056 (July 2018), p. 012031. DOI: 10.1088/1742-6596/1056/1/012031.

[6] KM3NeT. *Album: Optical module*. [Online; accessed June 12, 2024]. URL: https://www.km3net.org/pictures-and-videos/picture-galleries/album-optical-module/.

[7] Sebastiano Aiello et al. "First observation of the cosmic ray shadow of the Moon and the Sun with KM3NeT/ORCA." In: *The European Physical Journal C* 83 (Apr. 2023). DOI: 10.1140/epjc/s10052-023-11401-5.

[8] Tommaso Chiarusi and Matteo Sanguineti. "Moon shadow in ANTARES." In: *EPJ Web of Conferences* 207 (Jan. 2019), p. 07007. DOI: 10.1051/epjconf/201920707007.

[9] M.âG. Aartsen et al. “Observation of the cosmic-ray shadow of the Moon with IceCube.” In: *Physical Review D* 89.10 (May 2014). ISSN: 1550-2368. DOI: 10.1103/physrevd.89.102004. URL: http://dx.doi.org/10.1103/PhysRevD.89.102004.